Rapid Communications

Encircling exceptional points as a non-Hermitian extension of rapid adiabatic passage

J. Feilhauer,[1,2,*] A. Schumer,[2] J. Doppler,[2] A. A. Mailybaev,[3] J. Böhm,[4] U. Kuhl,[4] N. Moiseyev,[5] and S. Rotter[2]

[1]*Institute of Electrical Engineering, Slovak Academy of Sciences, 841 04 Bratislava, Slovakia*

[2]*Institute for Theoretical Physics, Vienna University of Technology (TU-Wien), 1040 Vienna, Austria*

[3]*Instituto Nacional de Matemática Pura e Aplicada-IMPA, 22460-320 Rio de Janeiro, Brazil*

[4]*Institut de Physique de Nice, Université Côte d'Azur, CNRS, 06108 Nice, France*

[5]*Schulich Faculty of Chemistry and Faculty of Physics, Technion-Israel Institute of Technology, 32000 Haifa, Israel*

(Received 25 March 2020; revised 2 September 2020; accepted 2 September 2020; published 7 October 2020)

The efficient transfer of excitations between different levels of a quantum system is a task with many applications. Among the various protocols to carry out such a state transfer in driven systems, *rapid adiabatic passage* (RAP) is one of the most widely used. Here we show both theoretically and experimentally that adding a suitable amount of loss to the driven Hamiltonian turns a RAP protocol into a scheme for encircling an exceptional point including the chiral state transfer associated with it. Our work thus discloses an intimate connection between a whole body of literature on RAP and recent studies on the dynamics in the vicinity of an exceptional point, which we expect to serve as a bridge between the disjoint communities working on these two scenarios.

DOI: 10.1103/PhysRevA.102.040201

Already in the early years of quantum mechanics the question was discussed how to coherently transfer the population from one discrete energy level to another one [1,2]. Ever since, coherent transfer schemes have become indispensable tools in many different areas of physics and technology—from simple spin-flip operations in a magnetic field to the preparation of atoms with well-defined populations of their excited states [3]. A particularly efficient transfer scheme with an inherent robustness is "rapid adiabatic passage" (RAP) [4–8]. While RAP is *rapid* enough to avoid any decoherence mechanism to kick in, it is *adiabatic* in the sense that the external drive is smoothly turned on and off to keep the system in an instantaneous eigenstate of its time-dependent Hamiltonian. Since the Hamiltonian of the system must be the same before and after the external driving sequence, any initial state follows a closed loop in the space of driving parameters. To achieve the desired population transfer, this closed loop must lead through an eigenvalue crossing at a degeneracy, also known as "diabolic point" (DP) or "conical intersection" [9].

In recent years, interest has been growing in non-Hermitian systems with controlled gain and loss that exhibit a wealth of unconventional and often surprising phenomena [10–16]. The focus of the community's attention currently revolves around the degeneracies that the corresponding non-Hermitian Hamiltonians give rise to. At these so-called "exceptional points" (EPs), not only the complex eigenvalues of this effective Hamiltonian coincide (in both their real and imaginary parts), but also their corresponding eigenvectors become parallel [17–29]. Another key feature of non-Hermitian systems is their dynamics: even when the time evolution is arbitrarily slow, the adiabatic transport along the eigenvalue surfaces may break down at sudden nonadiabatic jumps during a state's dynamical evolution [30–40]. One of the most surprising effects based on this breakdown of adiabaticity is a chiral state transfer: by continuously evolving two parameters along a closed loop around an EP, the final state at the end of the loop depends only on the encircling direction [clockwise (CW) vs counterclockwise (CCW)], but not on the initial state. This interesting and robust effect has meanwhile been demonstrated in a number of different experimental platforms [41–46].

The main goal of this Rapid Communication is to uncover a fundamental connection between RAP at a DP and the chiral state transfer at an EP. As we will demonstrate both theoretically and experimentally, these two transfer protocols are intimately connected in the sense that a RAP scheme in Hermitian systems results directly in the chiral encircling of an EP when losses are added appropriately. In other words, RAP and EP encircling are two sides of the same coin—an insight expected to create a much deeper understanding of how problems that have previously been studied with RAP carry over to the non-Hermitian domain and vice versa.

Our starting point is a general two-level system as described by the following simple 2×2 effective Hamiltonian,

$$\mathcal{H} = \frac{1}{2}\begin{bmatrix} -\Delta - i\gamma & \Omega \\ \Omega & \Delta + i\gamma \end{bmatrix}, \tag{1}$$

with the detuning Δ, the coupling strength Ω, and the loss or gain value γ entering the two eigenvalues $\lambda_\pm = \pm\lambda$ with $\lambda = \sqrt{(\Delta + i\gamma)^2 + \Omega^2}/2$. The dynamical evolution of the level amplitudes c_1 and c_2 is governed by the Schrödinger equation,

$$i\frac{\partial}{\partial t}\begin{pmatrix} c_1 \\ c_2 \end{pmatrix} = \mathcal{H}(t)\begin{pmatrix} c_1 \\ c_2 \end{pmatrix}, \tag{2}$$

where Δ and Ω in Eq. (1) are smoothly adjusted with time.

*juraj.feilhauer@savba.sk

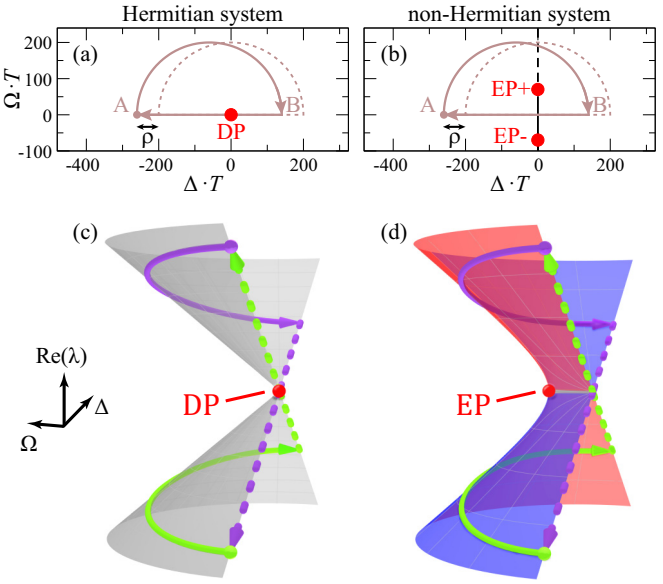

FIG. 1. (a), (b) Clockwise adiabatic passage along a semicircular trajectory ($A \to B$) followed by a straight return path ($B \to A$) at zero coupling ($\Omega = 0$). In the Hermitian case (a) the closed loop crosses a DP, whereas in the non-Hermitian case (b) it encircles one EP (labeled EP+). The parameter ρ measures the loop offset from the center position at $\Delta = 0$, i.e., the necessary loop asymmetry for a successful chiral state transfer in the non-Hermitian system. In (c) and (d) we show the corresponding parametric state evolution by the arrows on the real part of the eigenvalue surfaces (for simplicity, dynamical effects such as nonadiabatic jumps are excluded here; see Fig. 2 for comparison). Violet (dark-gray) and green (light-gray) arrows show the state evolution starting on the first and second level, respectively. The red (gain) and blue (loss) regions in (d) correspond to $\mathrm{Im}\lambda_\pm > 0$ and $\mathrm{Im}\lambda_\pm < 0$, respectively.

In the Hermitian case without loss or gain ($\gamma = 0$) the eigenenergy surfaces $\lambda(\Delta, \Omega)$ in the parameter space (Δ, Ω) form a pair of conical sheets connected at a DP located at $\Delta = \Omega = 0$ [see Fig. 1(c)]. In Figs. 1(a) and 1(c) we demonstrate the adiabatic switch of the level populations associated with the RAP protocol by following a closed loop starting at point A located at $\Omega = 0$. First we pass through a semicircular (SC) trajectory between points A and B ($\mathrm{SC}_{A\to B}$) where the coupling Ω is switched on and off while the detuning Δ is simultaneously swept through the resonance at $\Delta = 0$. The closing of the loop is achieved by connecting B with A along a linear (L) path ($\mathrm{L}_{B\to A}$) by sweeping the detuning backwards at zero coupling through the DP. The important point to observe is that the desired final state at the end of the closed loop is realized already at point B such that RAP usually terminates already there and the fictitious linear path $\mathrm{L}_{B\to A}$ is omitted (see Supplemental Material (SM) [47] for more details). Since the same reasoning also holds when the semicircular loop is orbited in counterclockwise direction, the RAP protocol described above generates a symmetric eigenstate switch where any initial eigenstate is adiabatically exchanged at the end of the evolution regardless of the loop's orbiting direction.

In a next step, we make the Hamiltonian in Eq. (1) non-Hermitian by introducing a finite loss-gain value $\gamma > 0$ in its diagonal elements. With one level now being amplified and the other one being attenuated, the eigenvalues $\lambda_\pm$ become complex with the real part representing the energy and the imaginary part defining the rate of amplification (for $\mathrm{Im}\lambda_\pm > 0$) or attenuation (for $\mathrm{Im}\lambda_\pm < 0$) of the corresponding eigenvectors [red and blue regions in Fig. 1(d)]. The DP from the Hermitian case splits into a pair of two EPs located at $\Delta = 0$ and $\Omega_{\mathrm{EP}\pm} = \pm\gamma$, where both the eigenvalues $\lambda_\pm = 0$ and the eigenvectors of Eq. (1) coalesce. As shown in Fig. 1(b), due to the symmetric splitting of the DP, one of the two EPs (at $\Omega_{\mathrm{EP}+} = \gamma$) is now located inside the closed parametric RAP loop whereas the second EP is not. The finite value of the loss-gain parameter γ thus transforms the conventional RAP scheme into a protocol for EP-encircling.

The topology of the energy eigensheets in the non-Hermitian system is shown in Fig. 1(d). On these Riemann sheets a purely *parametric* evolution along the same semicircular RAP loop as in the Hermitian case also leads to the same symmetric state switch that RAP gives rise to [compare Figs. 1(c) and 1(d) for the clockwise encircling direction] [15,24,26]. However, the fact that the *dynamic* state evolution of this non-Hermitian system is not necessarily adiabatic, leads to the asymmetric (chiral) state transfer associated with a loop around an EP [30–40,40–46]. In this case, the final state of the evolution depends only on the encircling direction and is independent of the initial state.

In Figs. 2(a)–2(d) we now provide the detailed numerical results for the fully *dynamical* state evolution for both the Hermitian and the non-Hermitian case. In both situations the level populations show the expected symmetric vs asymmetric state exchange also when the fictitious straight line path across the resonance at $\Delta = \Omega = 0$ is omitted and the evolution is restricted to just the semicircular RAP loop parametrized as $\Omega_{\mathrm{SC}}(t) = r\sin(\pi t/T)$ and $\Delta_{\mathrm{SC}}(t) = \mp r\cos(\pi t/T) + \rho$. We choose $r = 2$ as the radius of the semicircle, $\rho = -0.6$ as its horizontal offset, $T = 100$ as the encircling period, and the $\mp$ sign in $\Delta_{\mathrm{SC}}(t)$ defines the CW and CCW orbiting directions. The inversion of the level population is described by the quantity $p(t) = [|c_1(t)|^2 - |c_2(t)|^2)/(|c_1(t)|^2 + |c_2(t)|^2]$, where $p = \pm 1$ represent the cases where only the first or the second level is occupied, respectively. The violet (dark-gray) curves in the top and middle rows of Fig. 2 correspond to the evolution for the first level being initially populated [initial conditions $c_1(0) = 1$ and $c_2(0) = 0$] and the green (light-gray) curves for the second level initially populated [$c_1(0) = 0$ and $c_2(0) = 1$].

Consider first Figs. 2(a) and 2(b) (left column), where one can clearly see the successful operation of RAP: the evolution along $\mathrm{SC}_{A\to B}$ inverts the level populations for both orbiting directions and initial states [for more details on the conditions of adiabaticity see SM [47]]. In Figs. 2(c) and 2(d) (right column) the corresponding non-Hermitian evolution along the same path is depicted: one immediately sees that adiabaticity breaks down and nonadiabatic transitions arise that lead to a rapid transfer of populations towards the eigenvector with gain. The first such jump occurs for both orbiting directions at $t \approx 10$ [see violet curves in Figs. 2(c) and 2(d)]. The ensuing evolution is almost identical for both initial states and orbiting directions as it adiabatically follows the amplified instantaneous eigenvector (see also Fig. S3 in the SM [47]). However, as the $\mathrm{Im}\lambda = 0$ line (black dashed line) is crossed, the

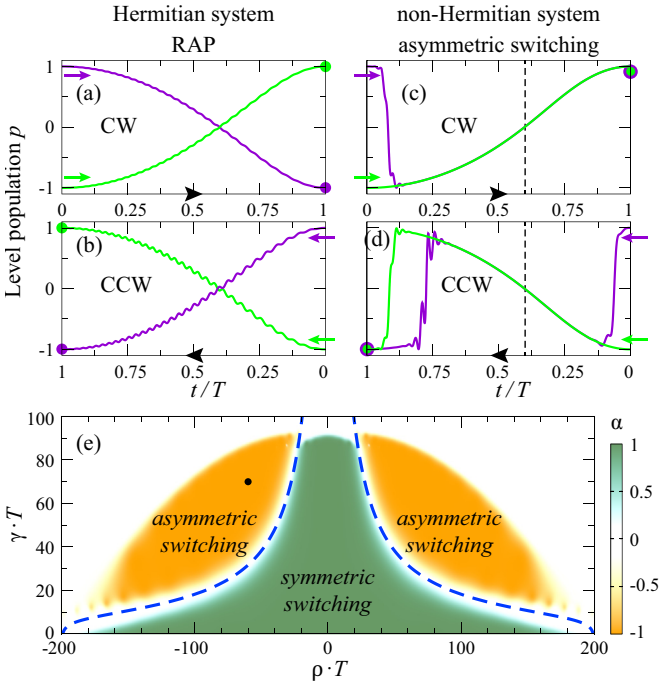

FIG. 2. (a)–(d) Dynamical evolution of the two-level populations governed by Eq. (2) tracked along the semicircular path ($SC_{A\to B}$) in Fig. 1 for the Hermitian (left panels) and non-Hermitian system (right panels, $\gamma = 0.7$). The numerical evolution of the level population p is initialized (at $t = 0$) in the first [violet (dark-gray) curves] and second level [green (light-gray) curves]. The arrows indicate the CW and CCW orbiting direction and the black dashed lines mark the position of the $\mathrm{Im}\lambda = 0$ line. Violet (dark-gray) and green (light-gray) dots mark the experimental values of mode populations p_n from waveguide data in Fig. 4. The bottom panel (e) shows a map of the state switch asymmetry when numerically following $SC_{A\to B}$ as a function of the loop offset ρ and the loss-gain value γ. The shown switching parameter α takes on its limiting values 1 (-1) for a symmetric (asymmetric) switch as in RAP (as in the chiral state transfer). Blue dashed line: transition from symmetric to asymmetric state transfer [see Eq. (4)]. Black dot: parameters of the semicircular loop in Fig. 1(b).

imaginary part of the eigenvalues changes sign. As a result, the state vector now follows the lossy eigenstate such that another nonadiabatic jump can occur. The onset of a potential nonadiabatic transition is, however, always delayed with respect to the sign change of $\mathrm{Im}\lambda$ [36], such that the remaining time of the loop decides whether or not the transition takes place. When the $\mathrm{Im}\lambda = 0$ line is crossed asymmetrically in time for the two orbiting directions in a way that, e.g., the delay time is longer than the remaining loop time in CW direction [Fig. 2(c)] but shorter than the remaining loop time in CCW direction [Fig. 2(d)], the state transfer shows the characteristic chiral behavior. This observation explains why a finite offset ρ of the semicircular loop with respect to the position of the $\mathrm{Im}\lambda = 0$ line (black dashed line) is required to induce this asymmetry.

To quantify the effect of the loop offset ρ on the asymmetry of the state switch, we introduce a measure $\alpha \in [-1, 1]$ that reflects the faithfulness of the symmetric ($\alpha = 1$) and asymmetric state transfer ($\alpha = -1$) and that highlights the boundaries between those two regimes ($\alpha = 0$). For this purpose we first multiply the values of the level population p at the beginning and end of the evolution as $S_j = p_j(t = 0) \times p_j(t = T)$, where the index $j = 1, 2$ labels which level is populated initially. This quantity S_j equals -1 if the eigenstate at the end is different from the initial one or $+1$ if the state vector returns back to the initial level. For the state switching in the CW and CCW encircling direction, the parameter α is then defined as follows,

$$\alpha = \left(S_1^{\mathrm{CW}} S_2^{\mathrm{CW}} + S_1^{\mathrm{CCW}} S_2^{\mathrm{CCW}} + S_1^{\mathrm{CW}} S_1^{\mathrm{CCW}} + S_2^{\mathrm{CW}} S_2^{\mathrm{CCW}}\right)/4. \quad (3)$$

A map of α as a function of ρ and γ is plotted in Fig. 2(e). The dark-green region centered around $\rho = 0$ defines the parameters where the evolution along the semicircular loop yields a symmetric switch. Albeit symmetric, the evolution is here not necessarily adiabatic since two subsequent nonadiabatic jumps during the EP encirclement would yield the same output eigenvector as a fully adiabatic passage [compare, e.g., violet (dark-gray) curves in Figs. 2(b) and 2(d)]. The symmetric and fully adiabatic evolution (as in RAP) is possible only for $\gamma \ll 1$. As discussed above, introducing a sufficient asymmetry ρ of the loop position with respect to the $\mathrm{Im}\lambda = 0$ line leads to the asymmetric switching (orange regions). Using the theory of stability loss delay [36] we estimate analytically the critical loss rate γ_c needed to transition from symmetric to asymmetric switching for $\gamma \ll r$,

$$\gamma_c \simeq \frac{2r}{T|\rho|} \ln\left[\frac{2T(r^2 - \rho^2)}{\pi r}\right]. \quad (4)$$

This estimate derived in detail in SM [47] is shown as a blue dashed line in Fig. 2(e) and accurately reproduces the numerically calculated crossover.

Reconsidering experimental RAP protocols that are always slightly non-Hermitian due to inevitable losses to the environment, we may thus conclude that RAP is typically realized as an EP encirclement with a sufficiently small loss contrast between the eigenmodes ($\gamma \ll \gamma_c$). In turn, simply increasing the loss contrast ($\gamma > \gamma_c$) at a sufficient offset value $|\rho|$ produces the chiral state transfer. For even larger values of γ and $|\rho|$ the evolving states eventually all yield $\alpha = 0$ [white region in Fig. 2(e)] since they all collapse into the gain eigenstate, regardless of the initial configuration and orbiting direction.

Our next aim is to demonstrate the fundamental connection between RAP and the chiral state transfer experimentally. We choose for this purpose a bimodal waveguide (WG) for microwaves in which the encircling of an EP and the associated chiral state transfer have recently been implemented [41]. In the following, we show that the same waveguide as used in [41] generates the symmetric RAP state switch, when a strong absorber that was placed inside the waveguide as part of the non-Hermitian EP-encircling protocol is simply removed. These results confirm the main message of this Rapid Communication, i.e., that the insertion or removal of losses alone can turn a RAP scheme into a recipe for EP encircling or vice versa.

The transmission of microwaves through the bimodal waveguide of length L and width W can be modeled by the Schrödinger equation (2) with the longitudinal coordinate x playing the role of time. The coupling

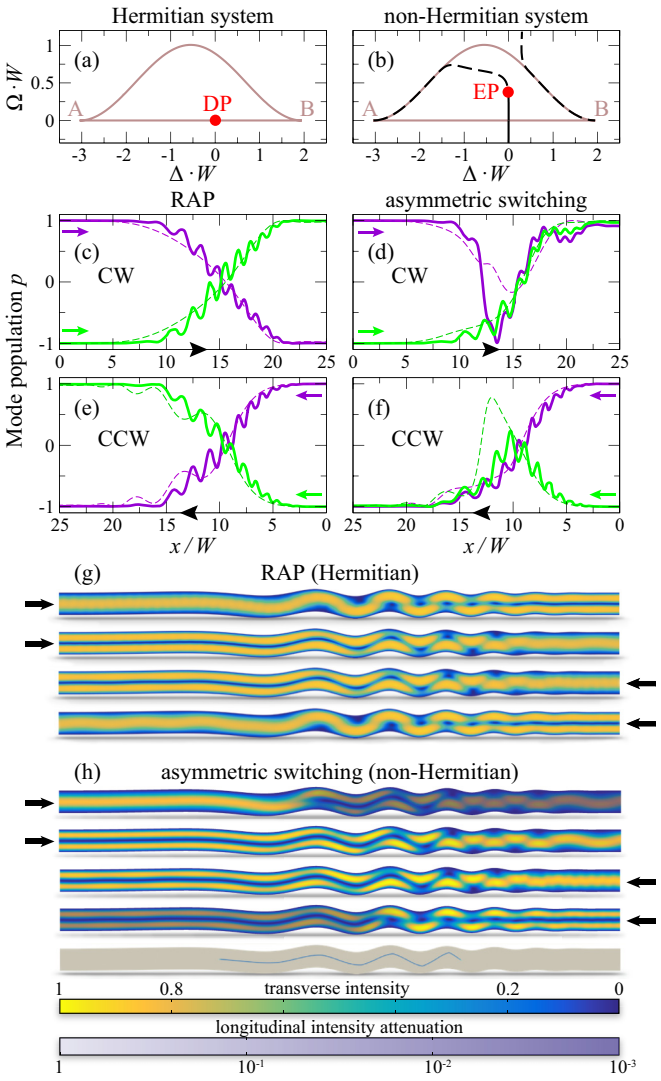

FIG. 3. Numerically calculated mode populations in the bimodal waveguide for $\omega W/\pi c = 2.6$ without (left column) and with absorber (right column). The top row shows the closed loops in parameter space which cross the DP in the case of an empty waveguide and enclose the EP in the case of a waveguide with absorber. Black dashed line in (b) marks the position of the $\mathrm{Im}\lambda = 0$ line. Panels (c)–(f) show the mode populations of microwaves injected into the waveguide from left and right (see arrows), calculated numerically (thick solid lines) and semianalytically (thin dashed lines). Panel (g) shows how the numerical field intensities of the transverse modes switch during the RAP protocol in the empty waveguide (arrows: injection). Similarly, panel (h) reproduced from [41] shows the numerical field intensities for the asymmetric switching, where the longitudinal attenuation along the waveguide is shown as an overlay (see color bars at the bottom). The foam absorber contained in this waveguide is sketched as a thin blue curve in the image right above the color bars.

between the modes is provided by the simultaneously oscillating waveguide boundaries [see Figs. 3(g) and 3(h) for an illustration] defined by the function $\xi(x) = \sigma \sin(k_b x)$ with amplitude σ and $k_b = k_1 - k_2 + \delta$, where δ represents the detuning from the resonant forward scattering at $\delta = 0$. As shown in detail in [41,47], the modal amplitudes are governed by an x-dependent Hamiltonian similar to Eq. (1), where the parameter σ is equivalent to Ω and δ is directly related to Δ. In order to reduce the backscattering of the microwaves at the start and end points A, B, we modify the semicircular RAP loop from Fig. 2 to the bell curve shown in Figs. 3(a) and 3(b) with the corresponding waveguide boundary modulation given by $\sigma(x) = \sigma_0[1 - \cos(2\pi x/L)]/2$ and $\delta(x) = \pm\delta_0(2x/L - 1) + \rho$ for $\delta_0 W = 1.25$, $\rho W = -1.8$, $\sigma_0/W = 0.16$, and $L/W = 25$ [41]. The CW and CCW propagation along this loop is equivalent to the left and right injection of microwaves into the waveguide.

The results of a full wave simulation [48–50] for the transmission across this bimodal waveguide are presented in Fig. 3 (see SM [47] for details). In the left column we consider the Hermitian case of this empty waveguide and observe a robust symmetric state switch for both initial modes and wave injection directions [see population inversions in Figs. 3(c) and 3(e) (thick solid lines)]. This behavior is also well reproduced by a semianalytical model based on Eq. (2) [see SM and Figs. 3(c) and 3(e) (thin dashed lines)]. The successful implementation of RAP is visible also directly through the microwave intensity profiles along the boundary-modulated waveguide shown in Fig. 3(g).

In the non-Hermitian case previously studied in [41], a thin but strong absorber with suitable shape is placed inside the waveguide to produce a sufficiently large loss contrast between the two modes (see SM [47]). To identify the position of the EP with respect to the chosen parameter loop, the definition of the waveguide Hamiltonian is extended to the whole parameter plane, involving both the localized absorber and the homogeneous dissipation in the waveguide cover plates (see SM [47]). As shown in Fig. 3(b), for the given waveguide geometry the EP is located inside the parametric loop and the evolution along the loop leads to the chiral mode switch for which the final states ejected at the two waveguide ends depend solely on the injection direction of the microwaves, but not on the injection profile [see Figs. 3(d), 3(f), and 3(h)] [41].

Our theoretical results from above demonstrate that RAP and chiral state transfer can be obtained within the same waveguide. For switching between these two scenarios, the only ingredient that needs to be changed is the presence of the absorber, which was already part of the non-Hermitian design in [41]. The waveguide considered there is built out of aluminum with dimensions $L \times W \times H = 2.38\ \mathrm{m} \times 5\ \mathrm{cm} \times 8\ \mathrm{mm}$ consisting of a 1.25-m-long region with undulating boundaries between two straight waveguide leads [41]. Microwaves with a frequency ν around 7.8 GHz are injected and detected by antennas located in the leads. Figure 4 shows the inter/intramode transmittances T_{mn} (from left to right) and T'_{mn} (from right to left) from mode m to mode n measured as a function of microwave frequency in the absence (left panel) and in the presence (right panel) of a thin foam absorber. As discussed already in [41], in the waveguide including the absorber the measured intensities satisfy $T_{11} \gg T_{12}, T_{21} \gg T_{22}$ and $T'_{12} \gg T'_{11}$, $T'_{22} \gg T'_{21}$, which is a hallmark of the chiral state transfer: both modes injected from the left (solid curves) leave the waveguide primarily in the first mode and both modes injected from the right (dashed curves) leave the waveguide primarily in the second mode. If, on the other hand,

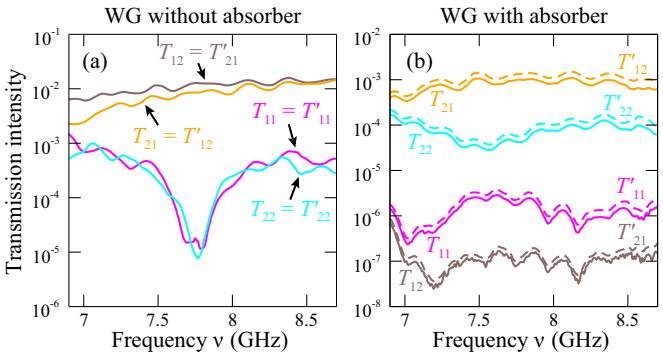

FIG. 4. Experimental transmission intensities in the microwave waveguide without (left panel) and with absorber (right panel). The solid and dashed curves correspond to the quantities of the left-to-right (T_{mn}) and right-to-left (T'_{mn}) transmission intensities from mode m into mode n. Data in (b) reproduced from [41]. The low transmission intensities in the WG without the foam absorber stem from the fact that most of the transmitted wave is not detected by the scanning antenna because of its weak coupling to the waveguide and its relatively small radius. Additionally, the radial symmetry of the input antennas' emission patterns causes half of the injected intensity to be lost already at the input (the intrinsic losses of the metallic WG are comparatively small). These spurious losses are not calibrated out in our measurements as they only reduce the global transmittance, while the relevant ratios of the individual mode transmittances are unaffected.

we remove the absorber from the waveguide, we observe that around the design frequency of $\nu = 7.8$ GHz the intermode transmittances are about three orders of magnitude larger than the intramode ones, which proves the successful operation of RAP. To compare these experimental results directly with our simple model from Eq. (1), we mapped these transmittances at $\nu = 7.75$ GHz to corresponding mode populations via $p_n = (T_{n1} - T_{n2})/(T_{n1} + T_{n2})$, $n = 1, 2$ and included them in Fig. 2 as violet (dark-gray) points for $n = 1$ and green (light-gray) points for $n = 2$ at the end of the corresponding loops. Our experimental values for p_n nicely correspond to the final states of the evolution in the general model, confirming the successful experimental implementation of our theoretical concepts.

In summary, we have demonstrated the intimate connection between RAP in Hermitian systems and EP encircling in non-Hermitian systems. Using analytical and numerical tools, we have shown explicitly that judiciously adding dissipative loss to a system that employs a RAP scheme generates a chiral transfer scheme involving the encircling of an EP. In the experiment we implemented these results in reverse order, starting from a boundary-modulated waveguide for microwaves inside of which a mode-specific absorber was placed [41]. In the presence of the absorber, chiral transmission is observed that depends primarily on the injection port (left or right), but not on the incoming mode configuration. When removing the absorber, however, we obtained the symmetric state switch of RAP between the incoming and outgoing modes on either side. Apart from providing a topical bridge between these two concepts, our results open up many possibilities to alternate between the Hermitian and the non-Hermitian variant of state transfer whenever desirable.

J.F. wishes to acknowledge the support of Grant No. VEGA 2/0162/18, of the Action Austria-Slovakia and the National Scholarship Programme of the Slovak Republic. A.S. and S.R. were partly supported by the European Commission under project NHQWAVE No. MSCA-RISE 691209 and by the Austrian Science Fund (FWF) under Project No. P32300 (WAVELAND). N.M. acknowledges the support of the Israel Science Foundation Grant No. 1661/19.

[1] L. Landau, Phys. Z. Sowjet. **2**, 46 (1932).
[2] C. Zener, Proc. R. Soc. London, Ser. A **137**, 696 (1932).
[3] L. Allen and J. Eberly, *Optical Resonance and Two-Level Atoms*, Dover Books on Physics (Dover, New York, 2012).
[4] F. Bloch, Phys. Rev. **70**, 460 (1946).
[5] M. M. T. Loy, Phys. Rev. Lett. **32**, 814 (1974).
[6] N. V. Vitanov, T. Halfmann, B. W. Shore, and K. Bergmann, Annu. Rev. Phys. Chem. **52**, 763 (2001).
[7] B. W. Shore, Acta Phys. Slovaca **58**, 243 (2008).
[8] V. Malinovsky and J. Krause, Eur. Phys. J. D **14**, 147 (2001).
[9] L. P. Yatsenko, S. Guérin, and H.-R. Jauslin, Phys. Rev. A **65**, 043407 (2002).
[10] L. Feng, R. El-Ganainy, and L. Ge, Nat. Photonics **11**, 752 (2017).
[11] R. El-Ganainy, K. G. Makris, M. Khajavikhan, Z. H. Musslimani, S. Rotter, and D. N. Christodoulides, Nat. Phys. **14**, 11 (2018).
[12] M.-A. Miri and A. Alù, Science **363**, eaar7709 (2019).
[13] Ş. K. Özdemir, S. Rotter, F. Nori, and L. Yang, Nat. Mater. **18**, 783 (2019).
[14] S. Longhi, Europhys. Lett. **120**, 64001 (2018).
[15] N. Moiseyev, *Non-Hermitian Quantum Mechanics* (Cambridge University Press, Cambridge, UK, 2011).
[16] K. Pichler, M. Kühmayer, J. Böhm, A. Brandstötter, P. Ambichl, U. Kuhl, and S. Rotter, Nature (London) **567**, 351 (2019).
[17] T. Kato, Perturbation Theory for Linear Operators (1966).
[18] W. D. Heiss, J. Phys. A: Math. Theor. **45**, 444016 (2012).
[19] W. D. Heiss, Phys. Rev. E **61**, 929 (2000).
[20] C. Hahn, Y. Choi, J. W. Yoon, S. H. Song, C. H. Oh, and P. Berini, Nat. Commun. **7**, 12201 (2016).
[21] S.-B. Lee, J. Yang, S. Moon, S.-Y. Lee, J.-B. Shim, S. W. Kim, J.-H. Lee, and K. An, Phys. Rev. Lett. **103**, 134101 (2009).
[22] T. Gao, E. Estrecho, K. Bliokh, T. Liew, M. Fraser, S. Brodbeck, M. Kamp, C. Schneider, S. Höfling, Y. Yamamoto *et al.*, Nature (London) **526**, 554 (2015).
[23] R. Lefebvre, O. Atabek, M. Šindelka, and N. Moiseyev, Phys. Rev. Lett. **103**, 123003 (2009).
[24] O. Atabek, R. Lefebvre, M. Lepers, A. Jaouadi, O. Dulieu, and V. Kokoouline, Phys. Rev. Lett. **106**, 173002 (2011).

[25] O. Latinne, N. J. Kylstra, M. Dörr, J. Purvis, M. Terao-Dunseath, C. J. Joachain, P. G. Burke, and C. J. Noble, Phys. Rev. Lett. **74**, 46 (1995).
[26] C. Dembowski, H.-D. Gräf, H. L. Harney, A. Heine, W. D. Heiss, H. Rehfeld, and A. Richter, Phys. Rev. Lett. **86**, 787 (2001).
[27] B. T. Torosov, G. Della Valle, and S. Longhi, Phys. Rev. A **87**, 052502 (2013).
[28] S. Ibáñez, S. Martínez-Garaot, X. Chen, E. Torrontegui, and J. G. Muga, Phys. Rev. A **84**, 023415 (2011).
[29] F. Mostafavi, L. Yuan, and H. Ramezani, Phys. Rev. Lett. **122**, 050404 (2019).
[30] R. Uzdin, A. Mailybaev, and N. Moiseyev, J. Phys. A: Math. Theor. **44**, 435302 (2011).
[31] M. Berry and R. Uzdin, J. Phys. A: Math. Theor. **44**, 435303 (2011).
[32] M. Berry, J. Opt. **13**, 115701 (2011).
[33] E.-M. Graefe, A. A. Mailybaev, and N. Moiseyev, Phys. Rev. A **88**, 033842 (2013).
[34] P. R. Kaprálová-Žďánská and N. Moiseyev, J. Chem. Phys. **141**, 014307 (2014).
[35] I. Gilary, A. A. Mailybaev, and N. Moiseyev, Phys. Rev. A **88**, 010102(R) (2013).
[36] T. J. Milburn, J. Doppler, C. A. Holmes, S. Portolan, S. Rotter, and P. Rabl, Phys. Rev. A **92**, 052124 (2015).
[37] A. U. Hassan, G. L. Galmiche, G. Harari, P. Li Kam Wa, M. Khajavikhan, M. Segev, and D. N. Christodoulides, Phys. Rev. A **96**, 052129 (2017).
[38] A. U. Hassan, B. Zhen, M. Soljačić, M. Khajavikhan, and D. N. Christodoulides, Phys. Rev. Lett. **118**, 093002 (2017).
[39] Y. Choi, C. Hahn, J. W. Yoon, S. H. Song, and P. Berini, Nat. Commun. **8**, 1 (2017).
[40] S. N. Ghosh and Y. D. Chong, Sci. Rep. **6**, 19837 (2016).
[41] J. Doppler, A. A. Mailybaev, J. Böhm, U. Kuhl, A. Girschik, F. Libisch, T. J. Milburn, P. Rabl, N. Moiseyev, and S. Rotter, Nature (London) **537**, 76 (2016).
[42] H. Xu, D. Mason, L. Jiang, and J. G. E. Harris, Nature (London) **537**, 80 (2016).
[43] J. W. Yoon, Y. Choi, C. Hahn, G. Kim, S. H. Song, K.-Y. Yang, J. Y. Lee, Y. Kim, C. S. Lee, J. K. Shin *et al.*, Nature **562**, 86 (2018).
[44] X.-L. Zhang, S. Wang, B. Hou, and C. T. Chan, Phys. Rev. X **8**, 021066 (2018).
[45] L. J. Fernández-Alcázar, H. Li, F. Ellis, A. Alú, and T. Kottos, Phys. Rev. Lett. **124**, 133905 (2020).
[46] Q. Liu, S. Li, B. Wang, S. Ke, C. Qin, K. Wang, W. Liu, D. Gao, P. Berini, and P. Lu, Phys. Rev. Lett. **124**, 153903 (2020).
[47] See Supplemental Material at http://link.aps.org/supplemental/10.1103/PhysRevA.102.040201 for analytical and numerical details on the state transfer as well as on microwave transmission through the waveguide with undulated boundaries.
[48] S. Rotter, J.-Z. Tang, L. Wirtz, J. Trost, and J. Burgdörfer, Phys. Rev. B **62**, 1950 (2000).
[49] F. Libisch, S. Rotter, and J. Burgdörfer, New J. Phys. **14**, 123006 (2012).
[50] B. Weingartner, S. Rotter, and J. Burgdörfer, Phys. Rev. B **72**, 115342 (2005).